Analysis of Rotor Fragment Impact on Ballistic Fabric Engine Burst Containment Shields

J. H. Gerstle*
Boeing Commercial Airplane Company, Seattle, Wash.

As a step toward a better understanding of engine burst containment and ascertaining practical shield requirements, a large deflection shell computer program has been modified to model fragment impact, simultaneously calculate the motion of the fragment and shield and predict perforation. Recent test data indicates that substantial savings in engine burst containment shield weight may be possible by the use of ballistic fabrics. In metal shields the dissipation of fragment kinetic energy is due to compressive and shear deformation in the impact region followed by extensive bending and stretching deformation due to structural excitation. In contrast, a fabric shield dissipates the energy almost wholly by tensile deformation. The mechanical energy is distributed relatively rapidly throughout the shield as a result of the fabric's high wave speed and membrane response. Encouraging results were found in analytical comparisons with experimental data.

Introduction

JET engine rotor failures may occur from fatigue (high and low cycle), material defects, assembly errors, and secondary causes such as bearing failures, overtemperature induced rubbing, and foreign object ingestion.

Commercial aviation statistics indicate that uncontained rotor fragments pose a potential, albeit very low probability hazard. However, the rate of uncontained failures (i.e., incidents in which fragments perforate the engine casing and/or nacelle has remained essentially unabated at approximately 30 per year over the last decade).[1-3]

Several approaches are being taken to reduce the probability of a catastrophic engine burst, including development of crack detection sensors and more damage-tolerant rotor materials. However, at least for the near future, aircraft designers will have to ensure aircraft safety by configuring the aircraft such that control and fuel systems, fuel tanks, critical structural components, and the cabin are protected by either redundant design with sufficient physical separation of critical components or by location outside the envelope of probable fragment trajectories.

The methodology presently available for high-velocity-impact protection has been principally developed for large length to diameter ratio projectiles such as bullets or meteoroids. This type of impact phenomena, in general, produces very localized damage and has led to the development of dense armor materials such as steels and ceramics which are not practical for extensive application to commercial aircraft. In contrast, gas turbine disk fragments or large blade fragments may not only be much more massive but will possess significant rotational energy.

Starting in 1964, NASA has been sponsoring an experimental research program with the objective of obtaining design data on the response of containment ring and ring sector deflection shields to blade and disk impact.[1,4] Since 1968, this program has been directed toward the development of methods for predicting theoretically the interaction behavior between fragments and the containment rings as well as the transient response of containment/deflection ring structures.[5-7]

In 1972 an experimental program was initiated at the Boeing Company to evaluate lightweight shields for engine fragment burst containment. The early tests primarily used different configurations made from a multi-layered "S" glass fabric.[8] Subsequent tests used similar shield configurations made from Kevlar 49† and Kevlar 29,† a fabric offering a very high strength to weight ratio and excellent ballistic impact properties. The engine fragment containment program was also then combined with an analytical effort whose objectives were to predict fragment trajectories and the dynamic response of structures to rotor fragment impact. The overall program depicted in Fig. 1 compliments the Boeing PANSIP[9] concept. Available engine failure and maintenance reports together with accident statistics are being reviewed and used to identify appropriate magnitudes of fragment sizes, velocities and translational and rotational energies associated with blade, rim, and sector fragments. Then for a specific system concept, the propulsion system trade studies will indicate the level of shield requirements.

The objective of the first phase of testing is to establish the general shield configuration, i.e., to evaluate candidate materials and shield shapes. (For example, both flat and corrugated fabric configurations have been tested, as have laminates of different materials.) These screening (shield configuration) tests are being performed in the Boeing Impact Mechanics Laboratory. Here the experimental technique is to use a powder gun to accelerate a steel projectile in the shape of either a steel cube or a rectangular cross section steel rod. Impact velocity and residual projectile velocity, if shield perforation occurs, are measured by electronic and witness sheet techniques. Some high speed photography has also been used for correlation with the theoretically predicted shield deformation with time. By varying projectile size, velocity, aspect ratio and target thickness, an empirical fit to the data can be made which serves as an inexpensive numerical method to predict shield weight test requirements for arbitrary combinations of screening test conditions. This data is also useful for correlation purposes with the analytical structural model as will be discussed subsequently. When the screening tests show satisfactory results, testing will be undertaken to test the containment shield as it may be installed e.g. as cowl segment. This second phase of testing will investigate installation considerations such as the effect of noise suppression and/or outer cowl backing materials, substructure heat shielding or simulated engine

Received August 5, 1974. The author is indebted to E. A. Schaal and E. Tjonneland for their support and to M. N. Aarnes, R. J. Bristow, and C. D. Davidson for their cooperation and advice.

Index categories: Aircraft Structural Design; Structural Dynamic Analysis, Airbreathing Propulsion.

*Senior Specialist Engineer, Propulsion Research Unit.

†Trademark for the aramid fiber manufactured by the E. I. DuPont De Nemours & Co., Wilmington, Del.

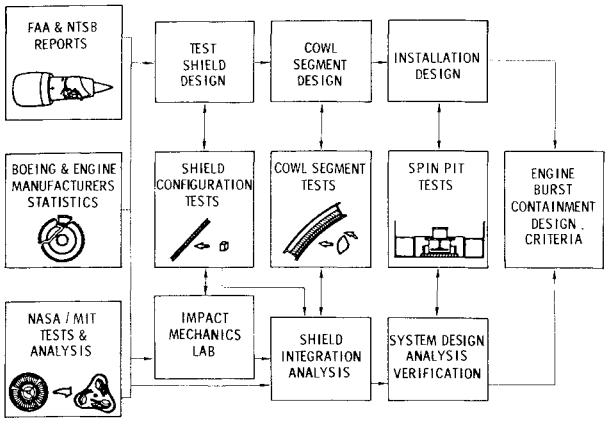

Fig. 1 Engine burst containment design criteria.

casing and attachments. Initial tests will continue to use powder gun driven steel projectiles. The powder gun tests have the advantage that they are much less expensive than spin pit tests, but have the disadvantage that the projectile will not have any rotational energy nor can it produce the same cutting effect as might occur from a rotating sharp edged rotor fragment. To verify the adequacy of the final installation design it is necessary to more realistically simulate an engine burst.

The final testing, as shown in Fig. 1, will therefore use spin pit test techniques.[4] To minimize the costs associated with spin pit tests, the structural response model will be used to predict the proposed nacelle containment design response. This analysis is expected to show whether the installation design will be adequate. If the structural model predictions are substantiated then analysis can also be used to predict the transient attachment loads and the total casing/containment shield/cowling/airframe energy absorption. The final product of this program will be engine burst containment design criteria. The design criteria will provide containment, installation, weight, and cost data.

Review of Test Data

Some results from the first phase of testing are shown in Fig. 2 together with other rotor burst data including spin pit test results. In this figure, total rotor fragment or simulated fragment energies are plotted against the areal weight density of the shield material sufficient to prevent perforation. The data has been taken from many sources, under widely different test conditions and so therefore this diagram is an over-simplified representation of *uninstalled* shield weights. Starting with the lower fragment energies, the titanium data represents the thickness found necessary to contain steel projectiles at normal incidence with dimensions simulating those of high-pressure compressor blades. The cluster of points around 300,000 in.-lb are taken from the NAPTC spin pit tests[4] for containment rings made of 4130 steel, filament wound "E" glass, a ballistic nylon-steel composite and TRIP steel (the apparently best material). At the high-energy end of the scale is shown the areal weight corresponding to the 1020 steel containment shell found to contain 90° sector disk fragments.[10] It is seen that these data points exhibit a remarkably consistent trend over three decades of energy levels despite the differences in fragment shapes, shield specific strengths and moduli, rotational velocities, and fragment frontal area/shield area ratios, to include most of the many important physical parameters in impact phenomena. Moreover, the test results differ in their proximity to containment thresholds. (A comparison to thicknesses used in actual design practice for blade protection

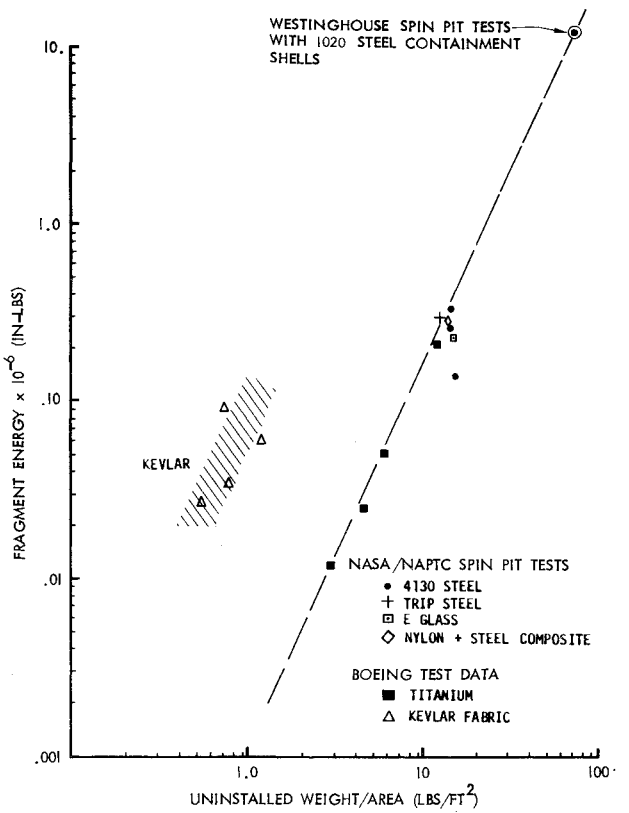

Fig. 2 Engine burst uninstalled shield weight estimates based on test data.

in commercial aircraft engines will show the metal weights in Fig. 2 to be relatively conservative.) Nonetheless the observation of this trend has served as a valuable preliminary design estimate of what weight penalties would be incurred if disk or blade fragments would have to be stopped by conventional metallic materials.

Also shown in Fig. 2 are results from the material configuration tests with Kevlar 49 and Kevlar 29. This data represents Kevlar shield areal weights which correspond to the observed ballistic limits.[11] While it must be emphasized that these results are still preliminary and indicate only uninstalled weight increments, the weight offsets shown in Fig. 2 for this fabric are very encouraging and warrant further research.

Analytical Approach

Analysis of the transient response of a fabric containment shield requires a computational method which allows large deformations of shell structures. Beam/ring response analysis is not adequate since the fabric containment shields must be supported and the ratio of the contact area to overall shield area may be very small.

The theoretical formulation and numerical techniques embodied in the PETROS codes[12] are readily adaptable for the purpose of a shield containment analysis computer program.‡ Since a comprehensive discussion of the basic theory can be found in Ref. 13, further discussion herein will be confined to the computational modifications required to predict fragment/fabric shield interactions.

‡The governing equations in PETROS 3 encompass the Kirchhoff shell approximations, large deflection elastic-plastic transient response and options for variable thickness, multilayer, multimaterial, hard bonded structures. Finite difference techniques are used to solve the resulting nonlinear equations.

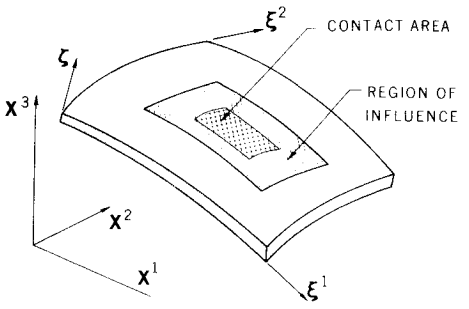

Fig. 3 Coordinate systems and effective instantaneous structural excitation area.

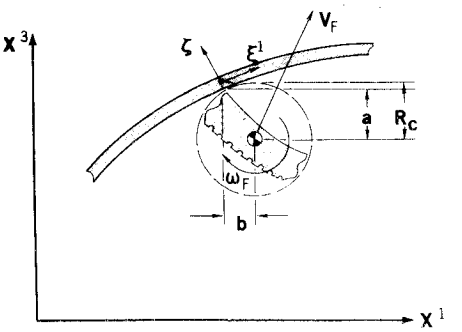

Fig. 4 Schematic of rotating fragment impinging on containment shield.

Impact Analysis

In the development of the theory for modeling arbitrary blade or disk fragment attacks on a fabric containment shield, emphasis has been placed on the development of a computational technique that incorporates the essential physical phenomena, but for design purposes can simulate an impact test adequately at a fraction of the cost of the experiment. This approach thus precludes the use of the two or three dimensional "material response" or stress wave codes which can model the full three dimensional deformation and time response of both fragment and shield (for continuous media).

To calculate the initial conditions for structural response at each occurrence of fragment/shield impact it is necessary to simultaneously calculate the trajectory of the fragment and the motion of the shield. At contact, the following assumptions are invoked. 1) The fragment remains rigid. 2) The impact process is perfectly inelastic which means that the relative velocity in the direction of fragment velocity between the fragment and shield at impact is zero. This implies a loss of kinetic energy. The idealization of the impact as perfectly elastic collision has been investigated, but as found in earlier studies,[6,7] it does not give significantly different results and also appears to be less realistic. 3) there is no relative sliding of the fragment along the shield, i.e., the coefficient of friction is infinite. (this assumption may become very inadequate at grazing impact angles); 4) the impact induced in-plane and transverse velocities at each node point vary spatially only with the embedded shell midsurface coordinates, ξ^1 and ξ^2 shown in Fig. 3. This assumption implies instantaneous equilibration in the transverse direction and is a good assumption for large spatial loading of a single layer continuum but is not very satisfactory for localized impact loading and/or weak bonded laminates, especially at very oblique impact angles. 5) For simplicity, the collisions are regarded to occur at the node nearest the center of contact with the fragment. 6) For purposes of calculating the velocity increments resulting from impact, the existence of an instantaneous equivalent rigid body shield mass M_s and shield velocity V_s is assumed. For convenience, the planes of rotation and translational velocity of the fragment are assumed to be in the X^2 plane as illustrated in Fig. 4.

The position of the fragment in the inertial Cartesian coordinate system (Fig. 3) is determined by the equations of motion

$$\begin{aligned} M_f\ddot{X}_f{}^1 &= 0 \\ M_f\ddot{X}_f{}^3 &= 0 \end{aligned} \tag{1}$$

where $\ddot{X}_f{}^1$ and $\ddot{X}_f{}^3$ are the acceleration components of the fragment's center of gravity and M_f is the fragment mass.

Rather than model in detail the exact shape and the angular rotation of a fragment (which in an actual uncontained engine burst would not be known), an effective radius of contact, R_c, is ascribed to the fragment as shown in Fig. 4. When the effective fragment radius exceeds the distance of the fragment c/g to the nearest node, a collision is assumed to have occurred. The successful application of this concept has been shown in the analysis of containment rings.[7]

Under these assumptions, conservation of translational momentum imposes

$$M_f(V_f{}^1 - V_{f0}{}^1) + M_s(V_s{}^1 - V_{s0}{}^1) = 0 \tag{2}$$

$$M_f(V_f{}^3 - V_{f0}{}^3) + M_s(V_s{}^3 - V_{s0}{}^3) = 0 \tag{3}$$

and conservation of angular momentum requires

$$I_f(w_f - w_{f0}) + M_s b(V_s{}^1 - V_{s0}{}^1) + M_s a(V_s{}^3 - V_{s0}{}^3) = 0 \tag{4}$$

where M_f is the mass of the fragment, I_f is the moment of inertia of the fragment about its centroid, w_f is the angular velocity of the fragment, and $V_f{}^1$, $V_f{}^3$, $V_s{}^1$, and $V_s{}^3$ are the translational velocities of the fragment and equivalent shield mass in the X^1 and X^3 coordinate directions, respectively, shown in Fig. 3. These quantities prior to impact are denoted by w_{f0}, $V_{f0}{}^1$, etc. The coordinates of the fragment's centroid relative to the impact node are denoted by a, b and are positive in the position shown in Fig. 4. It is assumed that no net angular momentum is imparted to the shield.

Imposing the requirement that the relative velocities of the fragment and shield are instantaneously zero upon impact provides two additional equations[14]:

$$V_s{}^1 - V_f{}^1 + bw_f = 0 \tag{5}$$

$$V_s{}^3 - V_f{}^3 - aw_f = 0 \tag{6}$$

Equations (2–6) may be solved directly to obtain

$$V_s{}^3 = \frac{c_1 + abc_3V_{s0}{}^3 - abc_3(c_2 + abc_3V_{s0}{}^3)}{c_4(M_s + M_f + a^2c_3) - (abc_3)^2} \tag{7}$$

where

$$c_1 = M_sV_{s0}{}^3 + M_fV_{f0}{}^3 + M_faw_{f0} + a^2c_3V_{s0}{}^3$$

$$c_2 = M_sV_{s0}{}^1 + M_fV_{f0}{}^1 + M_fbw_{f0} + b^2c_3V_{s0}{}^1$$

$$c_3 = M_sM_f/I_f$$

and

$$c_4 = M_s + M_f + c_3b^2$$

Having found $V_s{}^3$, the other velocity component may be

determined from

$$V_s{}^1 = c_2 - abc_3(V_s{}^3 - V_{s0}{}^3)/c_4$$

and the solution of w_f, $V_f{}^1$ and $V_f{}^3$ then follow trivially.

Material Behavior

The ballistic fabrics of current interest are orthogonally woven materials. The simplest material model thus idealizes a ballistic fabric as a single or multi-layered membrane capable of only supporting loads along the fibers. The fiber crossovers are treated as pin joints.[15] These fibers generally exhibit nonlinear stress-strain curves which may be expressed by

$$\sigma = E(\epsilon)\epsilon \tag{8}$$

where σ and ϵ are the components of the stress and strain and E is the elastic modulus. The shear stresses are assumed to be negligible although in reality the shear modulus and strength appear to be a function of the shear strain and are probably significant for tightly woven fabrics. Since some ballistic fibers are quite strain rate sensitive and appear to yield, later studies may need to characterize the fabrics by a viscoelastic or viscoplastic constitutive relation.[16]

Nodal Velocity Distribution

From both physical and numerical considerations it is undesirable to have the impulsive loading applied at a single node point. Physically, after impact the mechanical energy is transported by stress waves propagating in both the transverse and inplane directions. Since an incremental time step technique is used in the solution procedure, the region assumed to be perturbed by the impact is the fragment/shield contact area plus the shield area corresponding to that excited transversely by the impact-induced stress waves. This total area will be referred to as the impact region of influence and is shown in Fig. 3.§ The bounds for the region of influence for a fragment with a symmetric contact area can be estimated as:

$$\xi_R{}^1 = \xi_I{}^1 \pm (\xi_c{}^1 + c_T\Delta t)$$
$$\xi_R{}^2 = \xi_I{}^2 \pm (\xi_c{}^2 + c_T\Delta t) \tag{9}$$

where $\xi_I{}^1$ and $\xi_I{}^2$ are the coordinates of the node at the center of impact, $\xi_C{}^1$ and $\xi_C{}^2$ are the half lengths of the contact area, C_T is the transverse wave speed, Δt is the time step, and $\xi_R{}^1$ and $\xi_R{}^2$ are the effective half lengths of the region of influence. In the case of fibers, the transverse wave speed is not constant but depends on the fibers stress-strain state, i.e.,[16]

$$C_T = (\sigma/\rho(1 + \epsilon))^{1/2} \tag{10}$$

hence an appropriate C_T can only be roughly estimated. The shield material density is represented by ρ. For oblique fragment incidence, where there is significant in-plane momentum imparted to the shield, the transverse wave speed should be replaced by the longitudinal wave speed:

$$c_L = \left(\frac{1}{\rho}\frac{d\sigma}{d\epsilon}\right)^{1/2} \tag{11}$$

To avoid numerical difficulties which will arise if the mesh spacing is not small with respect to $\xi_R{}^1$ and $\xi_R{}^2$,[17] as many nodes as possible should be included in the region of influence.

The nodal velocities in the region of influence are determined from the effective shield mass and velocity. The effective shield mass is related to the region of influence by a thickness of

$$M_s = \frac{1}{2}\int_0^{\xi_R{}^2}\int_0^{\xi_R{}^1}\rho(\xi^1,\xi^2)h(\xi^1,\xi^2)[A(\xi^1,\xi^2)]^{1/2}d\xi^1 d\xi^2 \tag{12}$$

where h is the shield thickness and A is the determinant of the metric tensor associated with the deformed midsurface of the shield.[13] In the finite difference formulation the effective shield mass is determined from

$$M_s = \sum_i\sum_k m_{ik} \tag{13}$$

where m_{ik} is the mass centered at the mesh point $(\xi_i{}^1, \xi_k{}^2)$.

The nodal velocities $V_{ik}{}^j$ are then determined from the effective shield velocity by

$$M_s\dot{V}_s{}^j = \sum_i\sum_k m_{ik}\dot{V}_{ik}{}^j \tag{14}$$

with

$$V_{ik}{}^j = \begin{cases} V_I{}^j(1 - k_1n_1/N_1)(1 - k_2n_2/N_2) \\ 0 \text{ for } n_1 > N_1 \text{ or } n_2 > N_2 \end{cases} \tag{15}$$

where, for example, n_1 are the number of nodes in the coordinate direction away from the impact node, N_1 are the number of nodes in the ξ^1 direction corresponding to the half length of the contact area $\xi_C{}^1$, and $V_I{}^j$ are constants which can then be calculated analytically. For example, $K_1 = K_2 = 1$, $V_I{}^j = 1$ imposes a uniform velocity distribution. Based on two dimensional stress wave calculations using TOODY[18] a linear velocity gradient; e.g., $K_1 = K_2 = \frac{1}{3}$, appears to be more realistic than the uniform velocity idealization.

Solution Procedure

The flow diagram shown in Fig. 5 illustrates the numerical procedure used to predict the motion of the fragment and shield. For given initial conditions of fragment angular velocity, translational velocity and incidence angle the post-impact velocities of the fragment and shield are calculated as discussed above. Next, the nodal displacement components for the first time increment, $t = \Delta t$, are found from the nodal velocities. The midsurface geometric quantities at each mesh point are then calculated from the displacements, followed by the strain increments and then the stresses. A stress failure criterion is evaluated to

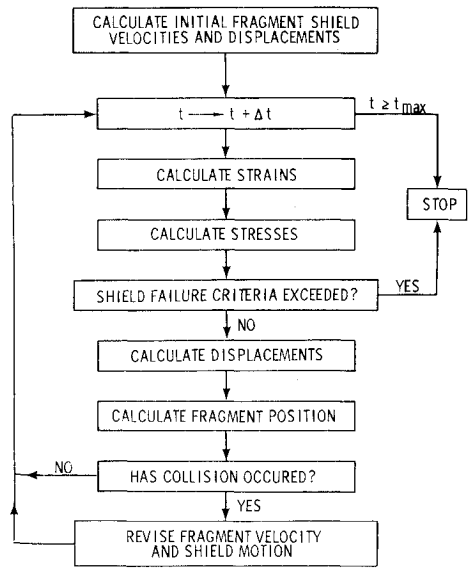

Fig. 5 Solution procedure.

§In previous studies either only a single node[15] or adjacent nodes[6,7] were given impact induced velocity increments.

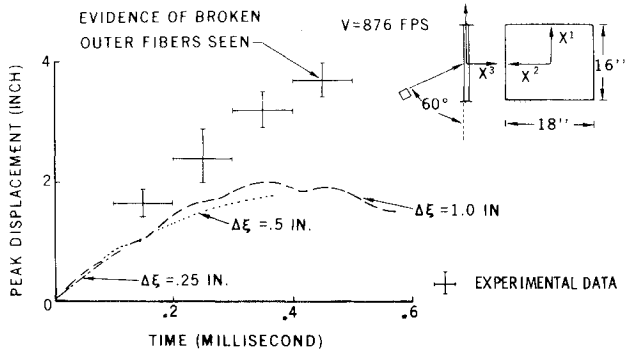

Fig. 6 Comparison of predicted and measured peak displacement in oblique impact material configuration test.

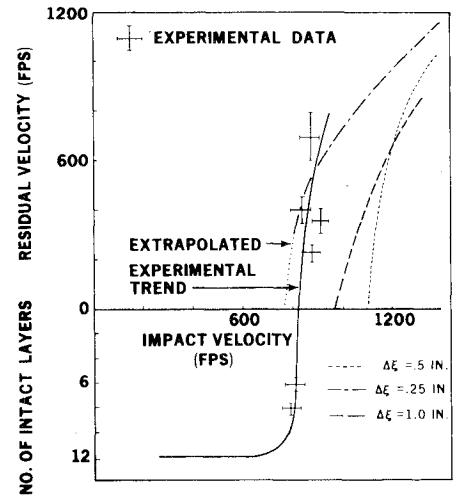

Fig. 7 Comparison of predicted and measured projectile residual velocities for 60° impact angle.

determine if the shield fibers could have ruptured. If not, the stresses are used to calculate stress resultants from which the new velocities are found by solving the equilibrium equation, thus specifying the new displacements. Next, the fragment's position is updated to correspond to the new time according to Eq. (1). A check is made to see if the effective fragment radius overlaps any mesh points. If not, the program flow cycle is repeated. Otherwise, a collision is assumed to have occurred and the impact analysis procedure is used to calculate velocity increments which are superimposed on the vibratory motion before entering a new cycle. The process ends either if a failure is predicted, a maximum time is reached, or a numerical stability condition is violated.

Results and Discussion

The measured peak displacement as a function of time from a material configuration test is shown in Fig. 6. In this experiment, a 1-in. nonrotating steel cube was shot at the center of a rectangular flat shield with an incidence angle of 60° with respect to the plane of the shield. The projectile velocity was reduced from 876 fps at impact to 250 fps after perforation. The shield was riveted to steel reinforcements at the top and bottom which in turn were bolted to a heavy steel frame. The shield was unattached at its two sides. A schematic of the test configuration may be seen in Fig. 6. The shield was composed of a number of layers. The first layer was a thin steel plate which may be regarded as simulating a support panel. This steel panel was experimentally found to reduce the residual projectile velocity by less than 10% for impact velocities above 800 fps. Twelve layers of Kevlar made up the rest of the shield. The deformation of the shield was obtained by high speed photography. Experimental uncertainties are shown by error bars on the experimental data points.

To compare results, the predicted peak displacement time histories are also shown in Fig. 6. In this analysis the shield was idealized as a single layer of fabric clamped at the top and bottom edges. Since the fabric layers are neither bonded nor quilted together, only the initial transient response prediction is meaningful.

Square meshes, with the node spacing indicated, and a time step satisfying the Courant stability condition were used in all cases. It was found necessary to smooth the stresses to minimize artificial numerical amplification due to the central differencing method and concentrated loading. The region of influence was 50% larger for the 1.0-in. grid spacing to ensure a sufficient number of initially excited node points.

The prediction of peak displacement as a function of time was found to not vary significantly with node spacing and was consistently lower than measured. Comparison of shield deflection profiles indicated that this was partly due to more localized deformations in the test. However the major shortcoming of the analysis was probably the lack of material data; i.e., a linear stress-strain curve based on the static mechanical fiber properties[19] was used. (The material is known to exhibit residual deformation under high speed impact.) With improved constitutive data the differences from the measured deformations are expected to be lessened.

It was noted that the fabric shield dissipates the energy almost wholly by tensile deformation. The mechanical energy is distributed rapidly throughout the fabric shield, relative to metal response, due to the fabric's high wave speed and membrane response. Transverse wave propagation, while not quantitatively predictable for a non-bonded structure, is attenuated extremely quickly. The in-plane compressive stresses physically will cause buckling, which in these analyses was not taken into account.

This dynamic behavior is in contrast to metal shields where the dissipation of the fragment's kinetic energy is initially due to compressive and shear waves. If perforation does not occur, then further dissipation of energy results from the bending and stretching deformation within response times on the same order of magnitude for equivalent structural excitation.

The results from a series of tests to determine the ballistic limit¶ of this configuration are shown in Fig. 7. The velocity range was chosen to provide energies characteristic of small compressor and turbine blades. It is seen that as impact velocities approach the ballistic limit of approximately 830 fps, the number of damaged (i.e., penetrated) fabric layers increases very rapidly for small increases in velocity. This may be interpreted as a load transfer process wherein after each layer is damaged the fragment applies the whole impulsive load to the remaining intact layers. Above the ballistic limit no appreciable loss of energy was discernible experimentally although the residual velocity is typically found in ballistic experiments to asymptotically approach a slope of roughly 45°.

To evaluate the effectiveness of the analytical method, the predicted residual velocities are again shown for various mesh spacings. The lack of convergence in the ballistic limit with decreasing mesh size is probably due to the relative coarseness of the shield discretization and the variation in the region of influence. A comparison of predicted residual velocities for 90° impacts gave similar results but with better convergence. It was noted in the earlier test configurations that rivets were failing at the higher impact velocities. The analysis also predicted the rivet

¶ The ballistic limit is the impact velocity at which the residual velocity is zero after perforation.

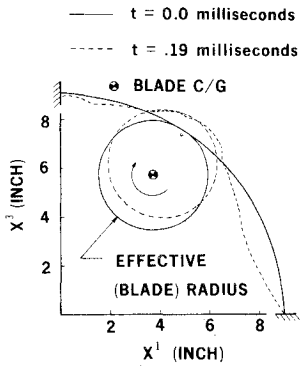

Fig. 8 Prediction of Kevlar cylindrical sector shield to small turbine blade impact.

failures, indicating the technique will be helpful in installation design. These results, while not altogether satisfactory, were sufficiently encouraging to continue the analytical development for engineering design purposes.

To illustrate the current state of the method, a Kevlar shield response is analyzed for the containment of the turbine rotor blade used as the example in Ref. 6. The blade weighs 0.084 lb and is assumed to be released with a translational velocity of 650 fps and a rotational rate of 15,000 rpm. Its inertia is 2.16×10^{-4} in.-lb-sec^2 and its effective fragment radius (c/g to tip length) is 2.2 in. A 90° sector, 9-in. radius, 4.5-in. axial length cylindrical panel was arbitrarily chosen for the shield configuration. The motion of the center of the shield is depicted in Fig. 8. One hundred eighty-six nodes were used to represent the panel with mesh spacings of approximately 0.5 in. For a simulated time of 1 msec, 12 min of computing time on the Boeing CDC 6600 are required. Present development efforts are being directed toward the modeling of transverse structural supports which would constrain the motion of the shield in the direction of the support.

Conclusions

An analytical simulation technique based on large deflection theory and on finite difference numerical methods has been applied to the prediction of rotor fragment containment shield configuration tests using newly developed ballistic fabrics. The correlation with experimental data showed fair agreement for the initial transient deflections and better agreement with the ballistic limit data for preliminary design purposes.

Further development of the analytical technique will help to minimize the number of test parameters and thereby the cost imposed by the necessity of experimentally validating an installation design. The principal investigative efforts should be threefold. First, refinements in the material model should be pursued to include fabric shear strength variation, strain rate sensitivity, fiber slippage, and nonlinearity, provided the appropriate mechanical property measurements can be made. The development of an empirical damage factor to account for stress concentrations due to transverse shear and/or initial tearing upon contact, should also be explored. Second, to enhance the capability of the analysis by modeling shields with stiffeners and branched structure, advantage should be taken of recent developments in large deflection finite element methods. Use of finite element techniques has been shown to give significantly better predictions of strain for comparable computer costs.[20] Third, it is possible that complex shields will evolve using some materials to blunt the fragments and distribute their momentum and other to disperse and absorb the kinetic energy, similar to the impedance mismatching techniques used in armor design. In some design cases, it may be necessary to back up the containment shield with noise attenuation or structural materials. Hence, for an analytical technique to be applicable to engine/nacelle design, multilayer, multimaterial response capability should be incorporated.

References

[1]Chiarito, P. T., "Status of Engine Rotor Burst Protection Program for Aircraft," NASA Aircraft Safety and Operating Problems Conference, SP-270, May 1971, Langley Research Center, NASA.

[2]DeLucia, R. A. and Mangano, G. J., "Rotor Burst Protection Program: Statistics on Aircraft Gas Turbine Failures that Occurred in Commercial Aviation During 1971," NAPTC-PE-12, DPR C-41581-B-4, Feb. 1973, U.S. Navy, NASA.

[3]Clarke, R. B., "Rotor Disk Burst Characteristics," Rept. 6-7670-RS-399, March 1973, Boeing Co., Seattle, Wash.

[4]Mangano, G. J., "Rotor Burst Protection Program—Phases VI and VII: Exploratory Experimentation to Provide Data for the Design of Rotor Burst Containment Rings," NASA DPR C-41581-B-1, NAPTC-AED-1968, March 1972, Naval Air Propulsion Test Center, Trenton, N.J.

[5]McCallum, R. B., "Simplified Analysis of Trifragment Rotor Disk Interaction with a Containment Ring," *Journal of Aircraft*, Vol. 7, May 1970, pp. 283–285.

[6]Wu, R. W. H. and Witmer, E. A., "Approximate Analysis of Containment/Deflection Ring Responses to Engine Rotor Fragment Impact," *Journal of Aircraft*, Vol. 10, Jan. 1973, pp. 28–37.

[7]Collins, T. P. and Witmer, E. A., "Application of the Collision—Imparted Velocity Method for Analyzing the Responses of Containment and Deflector Structures to Engine Rotor Fragment Impact," ASRL TR 154-8, CR-134494, Aug. 1973, MIT, Cambridge, Mass., NASA.

[8]Davidson, C. D. and Stachoviak, C. R., "Engine Rotor Burst Containment with "S" Glass Fabric—Phase I Report," Rept. T6-5799, Sept. 1973, Boeing Co., Seattle, Wash.

[9]Aarnes, M. N. and White, J. L., "Propulsion System and Airframe Structural Integration Program, PANSIP," this issue, pp. 234–241.

[10]Hagg, A. C., and Sankey, G. O., "The Containment of Disk Burst Fragments by Cylindrical Shells," *Journal of Engineering for Power*, Vol. 96, April 1974, pp. 114–123.

[11]Davidson, C. D., "Engine Burst Containment Shield Development (Phase II) in Kevlar Fabric," Rept. D6-41904, Dec. 1974, Boeing Co., Seattle, Wash.

[12]Atluri, S., Witmer, E. A., Leech, J. W., and Morino, L., "PETROS 3: A Finite-Difference Method and Program for the Calculation of Large Elastic-Plastic Dynamically-Induced Deformations of Multilayer Variable Thickness Shells," ASRL TR 152-2, BRL CR 60, Nov. 1971, MIT, Cambridge, Mass.

[13]Morino, L., Leech, J. W., and Witmer, E. A., "An Improved Numerical Calculation Technique for Large Elastic-Plastic Transient Deformations of Thin Shells," *Journal of Applied Mechanics*, Vol. 38, June, 1971, pp. 423–436.

[14]Goldsmith, W., *Impact: The Theory and Physical Behavior of Colliding Solids*, Ch. 2, Edward Arnold Ltd., London, 1960.

[15]Roylance, D., Wilde, A., and Tocci, G., "Ballistic Impact of Textile Structures," *Proceedings of the Army Symposium on Solid Mechanics*, Ocean City, Md., Oct., 1972.

[16]Cristescu, N., *Dynamic Plasticity*, Ch. 4, North-Holland Publ. Co., Amsterdam, 1967.

[17]Geers, T. L. and Sobel, L. H., "Analysis of Transient, Linear Wave Propagation in Shells by the Finite Difference Method," NASA CR-1885, Dec., 1971, Lockheed Missiles and Space Co., Palo Alto, Calif.

[18]Bertholf, L. D. and Benzley, S. E., "TOODY II: A Computer Program for Two-Dimensional Wave Propagation," SC-RR-68-41, Nov. 1968, Sandia Lab., Albuquerque, N. Mex.

[19]"Kevlar 49 Data Manual," E. I. DuPont De Nemours & Co., Wilmington, Del., 1974.

[20]Wu, R. W. H. and Witmer, E. A., "The Dynamic Response of Cylindrical Shells Including Geometric and Material Nonlinearities," *International Journal of Solids and Structures*, Vol. 10, Feb. 1974, pp. 243–260.